Electronic Research Archive

https://www.aimspress.com/journal/era

ERA, 34(3): 1413–1433.
DOI: 10.3934/era.2026064
Received: 19 December 2025
Revised: 22 January 2026
Accepted: 23 January 2026
Published: 11 February 2026

Research article

A linearized and maximum bound principle preserving finite difference scheme for the Allen–Cahn equation with logarithmic free energy

Baitong Ma, Huiying Hou, Qiuyi Tian and Tianliang Hou*

School of Mathematics and Statistics, Beihua University, Jilin 132013, China

* **Correspondence:** Email: htlchb@163.com.

Abstract: This study concentrates on the Allen–Cahn equation with logarithmic free energy, thereby proposing a second–order accurate finite difference scheme. The core design of the scheme adopts a linearized modified version of the classical leapfrog scheme for temporal discretization, combined with central differencing for spatial discretization. To further improve the numerical stability, a second–order stabilization term is systematically integrated into the discrete framework. A theoretical analysis reveals that under appropriate constraints on the time step size and stabilization parameter, the numerical solution strictly adheres to the maximum bound principle. A comprehensive stability analysis is performed in the maximum norm, and the corresponding error estimates are rigorously derived. Finally, numerical experiments are conducted to verify the correctness and effectiveness of the theoretical results.

Keywords: Allen–Cahn equation; leapfrog; finite difference method; maximum bound principle; error estimate

1. Introduction

In this paper, we consider the finite difference approximation of the following 1D Allen–Cahn equation:

$$\frac{\partial u}{\partial t} = \varepsilon^2 u_{xx} - F'(u),\ x \in (a,b),\ t \in (0,T], \tag{1.1}$$

$$u(x,0) = u_0(x),\ x \in [a,b], \tag{1.2}$$

$$u(a,t) = u(b,t) = 0,\ t \in (0,T], \tag{1.3}$$

where $\varepsilon > 0$ represents the interfacial width parameter, $T > 0$, and $F(u)$ is the following logarithmic potential:

$$F(u) = \frac{\theta}{2}[(1+u)\ln(1+u) + (1-u)\ln(1-u)] - \frac{\theta_c}{2}u^2.$$

Here,

$$0 < \theta < \theta_c,\ F'(u) = \frac{\theta}{2} \ln \frac{1+u}{1-u} - \theta_c u,\ F''(u) = \frac{\theta}{1-u^2} - \theta_c.$$

The diffuse interface phase–field method has emerged as a powerful tool to model mesoscopic morphological pattern formation and interface dynamics, thus attracting significant attention in recent years. A cornerstone of this approach is the Allen–Cahn equation (1.1), which is a mathematical model proposed by Allen and Cahn [1] in 1979 to describe such physical phenomena. Subsequently, Miranville and Quintanilla [2] generalized this equation in 2015, thereby substantially broadening its applicability to more complex physical processes, enriching its theoretical underpinnings, and providing robust support for subsequent applied research.

The numerical solution of the Allen–Cahn equation has been a subject of intensive study. Jeong et al. [3] conducted a comparative analysis of various numerical methods in 2016, thereby evaluating their accuracy, stability, and computational efficiency, thus offering valuable guidance for method selection in practical scenarios. Concurrently, Shin et al. [4] introduced a hybrid finite element method, further diversifying the finite element techniques available for this equation, enhancing the flexibility of numerical solutions, and complementing the findings of Jeong et al. [3]. Yang et al. [5] proposed and analyzed an efficient discontinuous Galerkin method tailored to the stochastic Allen–Cahn equation subjected to multiplicative noise. The method was constructed by combining the symmetric interior penalty discontinuous Galerkin finite element method for spatial discretization with the implicit Euler method for temporal discretization. Zhao and Guan [6] constructed and analyzed energy–stable weak Galerkin schemes for the mixed–form Cahn–Hilliard equation, with the energy stability of these schemes hinging on a newly defined discrete energy functional. Together, these works advanced the fundamental numerical methodology from distinct perspectives.

Stability and convergence of numerical methods are crucial to ensure the reliability of solutions to the Allen–Cahn equation. Feng and Prohl [7] pioneered a rigorous numerical analysis of such methods in 2003, thereby connecting them to the mean curvature flow and establishing a foundational framework for stability analyses. Building upon this, Feng et al. [8,9] investigated the nonlinear stability of implicit–explicit methods and proposed a stabilized Crank–Nicolson/Adams–Bashforth scheme, thus marking progress from analysis to method design. Tang and Yang [10] proved that implicit–explicit schemes can preserve the maximum bound principle, which is a key property to ensure the physical reasonableness of numerical solutions. Hou and Leng [11] performed a convergence analysis of the stabilized Crank–Nicolson/Adams–Bashforth finite difference scheme, while Hou et al. [12] designed a second–order maximum principle–preserving finite difference scheme for periodic boundary conditions, thereby continuously refining the theory of stability and convergence from multiple dimensions. More recently, Xu and Fu [13] proposed an unconditionally energy–stable scheme that also preserves the maximum principle, thus significantly enhancing computational efficiency. Shen and Yang [14] conducted further numerical approximation studies on both the Allen–Cahn and Cahn–Hilliard equations, thus contributing to a more comprehensive and systematic understanding of the numerical stability of the classical Allen–Cahn equation.

The space–fractional Allen–Cahn equation, often combined with logarithmic free energy to better align with the energy characteristics of real materials, is primarily employed to describe nonlocal diffusion processes. Hou et al. [15] laid the groundwork for numerical research on fractional equations by analyzing the fully discrete Crank–Nicolson scheme applied to the space–fractional Allen–Cahn

equation. Li et al. [16] proposed a Crank–Nicolson/Adams–Bashforth finite difference scheme to preserve the maximum boundary principle for the Riesz space–fractional Allen–Cahn equation, while Zheng et al. [17] introduced two linearized schemes, thus optimizing from different perspectives. Zhang et al. [18] designed and analyzed a high–order implicit–explicit Runge–Kutta scheme for the time integration of the Riesz space–fractional Allen–Cahn equation, which inherits the maximum conservation principle. Zhang and Yang [19] proposed a structural scheme for the space–fractional Allen–Cahn equation with logarithmic Flory–Huggins potential. Beyond the Allen–Cahn equation itself, He and Sun [20] studied the stability and convergence of the Crank–Nicolson/Adams–Bashforth scheme for the time–dependent Navier–Stokes equations, and He [21] further extended this research to nonsmooth initial data. The design principles of such schemes offer important insights to construct numerical methods for the Allen–Cahn equation, particularly its fractional variants, thus demonstrating cross–equation methodological synergy. Huang et al. [22] proposed an adaptive operator splitting finite element method, and Park et al. [23] designed an unconditionally stable splitting method, thus further optimizing computational efficiency and stability in complex scenarios.

In addition, finite element methods have been widely used to solve phase–field models such as the Allen–Cahn equation. In certain cases, these methods are enriched through the use of suitable basis functions. Li et al. [24] presented both the design and theoretical analysis of a second–order numerical method for the Allen–Cahn equation, which describes anti–phase domain coarsening in binary alloys, and further performed rigorous numerical validations to confirm its unconditional energy stability. Yang et al. [25] developed fourth–order, unconditionally structure–preserving temporal schemes for the Allen–Cahn equation and its conservative forms, thereby leveraging mass–lumping finite element spatial discretization along with the integrating factor Runge–Kutta method and stabilization strategies. Recently, Nudo [26] put forward two one–parameter families of quadratic polynomial enrichment schemes, which were designed to enhance the precision of the traditional Crouzeix–Raviart finite element method. The implementation of these enrichment strategies relied on two key components: weighted line integrals, which serve as the enriched linear functionals, and quadratic polynomial functions, which act as the enrichment basis. Nudo [27] developed a comprehensive framework to upgrade the Crouzeix–Raviart finite element. This framework integrated quadratic polynomial functions with three extra generalized degrees of freedom. To realize this goal, he derived a characterization theorem for the enriched degrees of freedom, thus laying the essential theoretical groundwork for the definition of a novel enriched finite element. Dell'Accio et al. [28] introduced quadratic and cubic polynomial enrichment methods for the classical Crouzeix–Raviart finite element, with the core aim of generating high–accuracy approximations within the enriched element spaces. For the quadratic enrichment, they added three weighted line integrals as supplementary degrees of freedom, while the cubic enrichment required the incorporation of seven such weighted line integrals.

Although Allen–Cahn models with logarithmic potential have been previously studied, our focus is on a particularly simple second–order discretization that is compatible with the singular logarithmic free energy through the discrete maximum bound principle. The maximum bound principle guarantee keeps the numerical solution in $[-\beta, \beta]$, which prevents encountering the logarithmic singularity and enables an L^∞–based analysis. The logarithmic potential is physically better motivated than the commonly used smooth polynomial double–well potential: it stems from mixing–entropy modeling and naturally enforces the admissible constraint $|u| < 1$, whereas polynomial potentials are globally smooth and do not intrinsically prevent nonphysical values.

Motivated by the works in [11,16], the present study focuses on developing alternative linear schemes that preserve the maximum bound principle for the Allen–Cahn equation. Specifically, we propose a linearized finite difference scheme that preserves the maximum bound principle for the Allen–Cahn equation with logarithmic free energy. First, we establish that the numerical solution satisfies the maximum bound principle. Subsequently, we derive an L^∞ error estimate by leveraging the boundedness of the numerical solution. The findings presented herein can be readily extended to two–dimensional and three–dimensional problems.

The remainder of this paper is structured as follows: in Section 2, the fully discretized scheme is detailed; Sections 3 and 4 are dedicated to discussions on the maximum bound principle and the L^∞ error estimate, respectively; and finally, several numerical experiments are conducted in the last section to validate the theoretical results.

2. The fully discretized scheme

We partition the interval (a, b) into a uniform mesh with the space step $h = (b - a) / (N + 1)$ and temporal step size $\tau = T/M$, where N and M are positive integers. Additionally, the set of grid points are denoted by $x_i = a + ih$ and $t_n = n\tau$ for $1 \le i \le N + 1$ and $0 \le n \le M$, and we use the notations $u^n = u(x, t_n)$ and $u_i^n = u(x_i, t_n)$. Define the following:

$$V_h = \{v : v = \{v_i\} \text{ is a grid function in } \{x_i = a + ih\}_{i=1}^N \text{ and } v_0 = v_{N+1} = 0\}.$$

For any $v = \{v_i\} \in V_h$, we define the pointwise maximum norm as follows:

$$\|v\| = \sqrt{h \sum_{i=1}^{N} v_i^2}, \ \|v\|_\infty = \max_{1 \le i \le N} |v_i|.$$

Hereinafter, we denote the discretization matrix by D_h, which is given by the following:

$$D_h := \frac{1}{h^2} \begin{bmatrix} -2 & 1 & & & \\ 1 & -2 & 1 & & \\ & \ddots & \ddots & \ddots & \\ & & 1 & -2 & 1 \\ & & & 1 & -2 \end{bmatrix}_{N \times N.}$$

Through straightforward calculations, we can obtain the following Lemma.

Lemma 2.1. *The matrix D_h satisfies the following properties:*
- *D_h is symmetric*;
- *D_h is negative definite (i.e., $U^T D_h U < 0$), for any nonzero $U \in \mathbf{R}^N$; and*
- *The elements of $D_h = (b_{ij})$ satisfy*

$$b_{ii} = -d < 0, \ d \ge \max_i \sum_{j \ne i} |b_{ij}|. \tag{2.1}$$

To solve Eq (1.1), we propose the following finite difference scheme:

$$\frac{U^{n+1}-U^{n-1}}{2\tau}+F'(U^{n-1})+F''(U^{n-1})(U^n-U^{n-1})+\gamma(U^{n+1}+U^{n-1}-2U^n)=\frac{\varepsilon^2 D_h(U^{n+1}+U^{n-1})}{2}, \quad (2.2)$$

for $n \geq 1$ with $\gamma \geq 0$. For the initial time step, we use the following nonlinear Crank–Nicolson finite difference scheme:

$$\frac{U^1-U^0}{\tau}+\frac{F'(U^1)+F'(U^0)}{2}=\frac{\varepsilon^2 D_h(U^1+U^0)}{2}, \quad (2.3)$$

where $U^0 := (u_0(x_1), u_0(x_2), \cdots, u_0(x_N))^T$ is the initial condition vector. Additionally, $U^n := (U_1^n, U_2^n, \cdots, U_N^n)^T$ represents the vector of numerical solution at nth level, and we define the following vector operations:

$$(U^n)^{.2} := ((U_1^n)^2, (U_2^n)^2, \cdots, (U_N^n)^2)^T, \ U^nV^n := (U_1^nV_1^n, U_2^nV_2^n, \cdots, U_N^nV_N^n)^T,$$

$$F'(U^n)=\frac{\theta}{2}\ln\frac{1+U^n}{1-U^n}-\theta_c U^n := \left(\frac{\theta}{2}\ln\frac{1+U_1^n}{1-U_1^n}-\theta_c U_1^n, \frac{\theta}{2}\ln\frac{1+U_2^n}{1-U_2^n}-\theta_c U_2^n, \cdots, \frac{\theta}{2}\ln\frac{1+U_N^n}{1-U_N^n}-\theta_c U_N^n\right)^T,$$

$$F''(U^n)=\frac{\theta}{1-(U^n)^{.2}}-\theta_c := \left(\frac{\theta}{1-\left(U_1^n\right)^2}-\theta_c, \frac{\theta}{1-\left(U_2^n\right)^2}-\theta_c, \ldots, \frac{\theta}{1-\left(U_N^n\right)^2}-\theta_c\right)^T.$$

3. The maximum bound principle

In this section, we will prove that the schemes (2.2) and (2.3) preserve the maximum bound principle.

Lemma 3.1. *Denote the following:*

$$g(x)=\frac{1}{3}x-2\tau\left(\frac{\theta}{2}\ln\frac{1+x}{1-x}-\theta_c x\right), \ x\in[-\beta,\beta].$$

Then, we have

$$|g(x)| \leq \frac{\beta}{3}$$

under the condition $\tau \leq \frac{1-\beta^2}{6(\theta-\theta_c+\theta_c\beta^2)}$.

Proof. Notice that

$$g'(x)=\frac{1}{3}-2\tau\left(\frac{\theta}{1-x^2}-\theta_c\right)$$

and

$$\max_{x\in[-\beta,\beta]} g(x)=g(\beta)=\frac{\beta}{3}, \ \min_{x\in[-\beta,\beta]} g(x)=g(-\beta)=-\frac{\beta}{3}.$$

If

$$\min_{x\in[-\beta,\beta]} g'(x)=\frac{1}{3}-2\tau\left(\frac{\theta}{1-\beta^2}-\theta_c\right)\geq 0,$$

then we can obtain

$$\tau \leq \frac{1-\beta^2}{6\left(\theta-\theta_c+\theta_c\beta^2\right)}.$$

It follows that $g(x)$ is monotone increasing over the interval $[-\beta,\beta]$. Thus, we complete the proof.

Theorem 3.2. *Assume that the initial value satisfies* $\max\limits_{x\in[a,b]}|u_0(x)| \le \beta$ ($\pm\beta$ *are the roots of* $F'(u)$ *and* $0 < \beta < 1$). *Then, the fully discrete scheme (2.2) preserves the maximum bound principle in the sense that* $\|U^n\|_\infty \le \beta$ *for all* $n \ge 0$, *provided that the time step size satisfies*

$$\tau \le \min\left\{\frac{2}{\theta_c}, \frac{h^2}{6\varepsilon^2}, \frac{1-\beta^2}{6\left(\theta-\theta_c+\theta_c\beta^2\right)}, \frac{1}{6\gamma}\right\}$$

and the stabilization parameter satisfies $\gamma \ge \frac{\theta-\theta_c\left(1-\beta^2\right)}{2-2\beta^2}$.

Proof. First, following the proof of Theorem 1 in [16], if the temporal step size τ satisfies $\tau \le \min\left\{\frac{2}{\theta_c}, \frac{h^2}{2\varepsilon^2}, \frac{1-\beta^2}{\theta-\theta_c+\theta_c\beta^2}\right\}$, then we can derive $\|U^1\|_\infty \le \beta$. We proceed with mathematical induction to complete the proof. Suppose the conclusion holds for $n = m-1$ and $n = m$ (i.e., $\|U^{m-1}\|_\infty \le \beta$ and $\|U^m\|_\infty \le \beta$). Below, we will check that this upper bound is also true for $n = m+1$.

Rewriting scheme (2.2) yields the following:

$$\begin{aligned}\left(I + 2\tau\gamma - \tau\varepsilon^2 D_h\right)U^{m+1} = {} & U^{m-1} + \tau\varepsilon^2 D_h U^{m-1} - 2\tau\gamma U^{m-1} - 2\tau F'\left(U^{m-1}\right) \\ & + 2\tau F''\left(U^{m-1}\right)U^{m-1} + 4\tau\gamma U^m - 2\tau F''\left(U^{m-1}\right)U^m.\end{aligned} \tag{3.1}$$

Suppose $\|U^{m+1}\|_\infty = |U_p^{m+1}|$. Then, $|U_p^{m+1}| \ge |U_j^{m+1}|$ for all $1 \le j \le N$. The *p–th* component of (3.1) is as follows:

$$\begin{aligned}& (1+2\tau\gamma)U_p^{m+1} - \frac{\tau\varepsilon^2}{h^2}\left(U_{p+1}^{m+1} - 2U_p^{m+1} + U_{p-1}^{m+1}\right) \\ = {} & \underbrace{\frac{1}{3}U_p^{m-1} + \frac{\tau\varepsilon^2}{h^2}\left(U_{p+1}^{m-1} - 2U_p^{m-1} + U_{p-1}^{m-1}\right)}_{} + \underbrace{\frac{1}{3}U_p^{m-1} - 2\tau\gamma U_p^{m-1}}_{} \\ & \underbrace{+ \frac{1}{3}U_p^{m-1} - 2\tau\left(\frac{\theta}{2}\ln\frac{1+U_p^{m-1}}{1-U_p^{m-1}} - \theta_c U_p^{m-1}\right)}_{} \\ & + 2\tau U_p^m\left[2\gamma - \left(\frac{\theta}{1-\left(U_p^{m-1}\right)^2} - \theta_c\right)\right] \\ & + 2\tau\left(\frac{\theta}{1-\left(U_p^{m-1}\right)^2} - \theta_c\right)U_p^{m-1} \\ = {} & : \sum_{i=1}^{5} I_i.\end{aligned} \tag{3.2}$$

Then, we know that $(1+2\tau\gamma)U_p^{m+1}$ and $-\frac{\tau\varepsilon^2}{h^2}\left(U_{p+1}^{m+1} - 2U_p^{m+1} + U_{p-1}^{m+1}\right)$ are non–positive or non–negative simultaneously; thus, we have the following:

$$\left|(1+2\tau\gamma)U_p^{m+1} - \frac{\tau\varepsilon^2}{h^2}\left(U_{p+1}^{m+1} - 2U_p^{m+1} + U_{p-1}^{m+1}\right)\right| \ge (1+2\tau\gamma)\left|U_p^{m+1}\right|. \tag{3.3}$$

If $\frac{1}{3} - \frac{2\tau\varepsilon^2}{h^2} \geq 0$, which implies $\tau \leq \frac{h^2}{6\varepsilon^2}$, then using (2.1) and $0 \leq |U_p^{m-1}| \leq \|U^{m-1}\|_\infty \leq \beta$, we obtain the following:

$$|I_1| \leq \frac{1}{3}\left|U_p^{m-1}\right| \leq \frac{1}{3}\beta. \tag{3.4}$$

If $\frac{1}{3} - 2\tau\gamma \geq 0$, then we have $\tau \leq \frac{1}{6\gamma}$. For I_2, since $0 \leq |U_p^{m-1}| \leq \|U^{m-1}\|_\infty \leq \beta$, it follows that

$$|I_2| \leq \left(\frac{1}{3} - 2\tau\gamma\right)\left|U_p^{m-1}\right| \leq \left(\frac{1}{3} - 2\tau\gamma\right)\beta. \tag{3.5}$$

Observe that each element of $\frac{1}{3}U_p^{m-1} - 2\tau\left(\frac{\theta}{2}\ln\frac{1+U_p^{m-1}}{1-U_p^{m-1}} - \theta_c U_p^{m-1}\right)$ is of the form

$$g(x) = \frac{1}{3}x - 2\tau\left(\frac{\theta}{2}\ln\frac{1+x}{1-x} - \theta_c x\right).$$

Applying Lemma (3.1) and $\|U^{m-1}\|_\infty \leq \beta$, we obtain the following:

$$\left|I_3\right| \leq \frac{\beta}{3}. \tag{3.6}$$

If $2\gamma - \left(\frac{\theta}{1-\left(U_P^{m-1}\right)^2} - \theta_c\right) \geq 0$ for $|U_p^{m-1}| \leq \beta$, then we have $\gamma \geq \frac{\theta - \theta_c\left(1-\beta^2\right)}{2-2\beta^2}$. We can see that

$$|I_4| = \left|2\tau U_p^m\left[2\gamma - \left(\frac{\theta}{1-\left(U_P^{m-1}\right)^2} - \theta_c\right)\right]\right| \leq 2\tau\beta\left[2\gamma - \left(\frac{\theta}{1-\beta^2} - \theta_c\right)\right]. \tag{3.7}$$

For I_5, applying $0 \leq |U_p^{m-1}| \leq \|U^{m-1}\|_\infty \leq \beta$ yields the following:

$$|I_5| = \left|2\tau\left(\frac{\theta}{1-\left(U_p^{m-1}\right)^2} - \theta_c\right)U_p^{m-1}\right| \leq 2\tau\left(\frac{\theta}{1-\beta^2} - \theta_c\right)\beta. \tag{3.8}$$

Taking the absolute value of (3.2) and using (3.3)–(3.8), we obtain the following:

$$\begin{aligned}(1+2\tau\gamma)\left\|U^{m+1}\right\|_\infty &\leq \frac{1}{3}\beta + \left(\frac{1}{3} - 2\tau\gamma\right)\beta + \frac{1}{3}\beta + 2\tau\left(\frac{\theta}{1-\beta^2} - \theta_c\right)\beta \\ &\quad + 2\tau\beta\left[2\gamma - \left(\frac{\theta}{1-\beta^2} - \theta_c\right)\right] \\ &\leq (1+2\tau\gamma)\beta.\end{aligned}$$

This completes the induction step, and the proof of the theorem is finished.

Remark 3.3. Without a loss of generality, we consider the 1D problem (1.1)–(1.3); however, the results regarding the discrete maximum bound principle and maximum–norm error in this work can be easily extended to 2D and 3D problems. In the numerical experiments, we separately present the numerical results for each dimension.

4. The maximum–norm error estimate

In this section, we will discuss the maximum–norm error estimate based on the maximum bound principle derived in Theorem 3.2. Let $C(\varepsilon, \theta, \theta_c, \gamma, T)$ be a positive constant which depends on $\varepsilon, \theta, \theta_c, \gamma, T$ and the regularity of the exact solution, but is independent of h and τ. Analogously, we can establish the definitions for the constants C, $C(\varepsilon)$, $C(\theta,\beta)$, $C(\varepsilon,\gamma)$ and $C(\varepsilon,\theta,\gamma)$. All such constants are independent of the discretization parameters (h,τ), and only depend on the continuous problem parameters and the final time T.

Theorem 4.1. *Assume that the exact solution $u(x,t)$ satisfies the regularity $u \in C^3([0,T]; C^4(\overline{\Omega}))$, and the initial value is smooth and bounded by β (i.e., $\max\limits_{x\in[a,b]} |u_0(x)| \le \beta$). If all the conditions specified in Theorem 3.2 are satisfied and $\tau \le \frac{h^2}{2(h^2\gamma+\varepsilon^2)}$, U^n $(2 \le n \le M)$ represents the solution to the fully discrete scheme (2.2), then the following error estimate holds:*

$$\|\boldsymbol{u}^n - U^n\|_\infty \le C(\varepsilon, \theta, \theta_c, \gamma, T)(\tau^2 + h^2),$$

where $\boldsymbol{u}^n := (u_1^n, u_2^n, \cdots, u_N^n)^T$ denotes the vector of the exact solution at the nth level.

Proof. First, we discretize (1.1) in space and time to obtain the following:

$$\frac{\boldsymbol{u}^{n+1} - \boldsymbol{u}^{n-1}}{2\tau} + \frac{\theta}{2}\ln\frac{1+\boldsymbol{u}^n}{1-\boldsymbol{u}^n} - \theta_c\boldsymbol{u}^n = \frac{\varepsilon^2 D_h\left(\boldsymbol{u}^{n+1} + \boldsymbol{u}^{n-1}\right)}{2} + \boldsymbol{\rho}^n, \tag{4.1}$$

where $\boldsymbol{\rho}^n := (\rho_1^n, \rho_2^n, \cdots, \rho_N^n)^T$, and $\left|\rho_i^n\right| \le C(\varepsilon)(\tau^2 + h^2)$, $1 \le i \le N$, $1 \le n \le M-1$.

Define the error vector $e^n = \boldsymbol{u}^n - U^n$ for $n = 0, 1, \cdots, M$. Subtracting (2.2) from (4.1) yields the following error equation:

$$\begin{aligned}
(1+2\tau\gamma)\,e^{n+1} - \tau\varepsilon^2 D_h e^{n+1} = {} & 4\tau\gamma e^n + 2\tau\left(\theta_c - \frac{\theta}{1-(U^{n-1})^2}\right)e^n \\
& + e^{n-1} - 2\tau\gamma e^{n-1} + \tau\varepsilon^2 D_h e^{n-1} + 2\tau\left(\frac{\theta}{1-(U^{n-1})^2} - \theta_c\right)e^{n-1} \\
& + 2\tau\left[\left(\frac{\theta}{2}\ln\frac{1+U^{n-1}}{1-U^{n-1}} - \theta_c U^{n-1}\right) - \left(\frac{\theta}{2}\ln\frac{1+\boldsymbol{u}^{n-1}}{1-\boldsymbol{u}^{n-1}} - \theta_c\boldsymbol{u}^{n-1}\right)\right] \\
& + 2\tau\left[\left(\frac{\theta}{2}\ln\frac{1+\boldsymbol{u}^{n-1}}{1-\boldsymbol{u}^{n-1}} - \theta_c\boldsymbol{u}^{n-1}\right) - \left(\frac{\theta}{2}\ln\frac{1+\boldsymbol{u}^{n}}{1-\boldsymbol{u}^{n}} - \theta_c\boldsymbol{u}^{n}\right)\right] \\
& + 2\tau\left(\frac{\theta}{1-(U^{n-1})^2} - \theta_c\right)\left(\boldsymbol{u}^n - \boldsymbol{u}^{n-1}\right) \\
& + 2\tau\gamma\left(\boldsymbol{u}^{n+1} - 2\boldsymbol{u}^n + \boldsymbol{u}^{n-1}\right) + 2\tau\boldsymbol{\rho}^n.
\end{aligned} \tag{4.2}$$

Suppose $\|e^{n+1}\|_\infty = |e_q^{n+1}|$, meaning that the maximum norm is attained at the q–th component. By

examining the q–th component of (4.2), we have the following:

$$\begin{aligned}
&(1+2\tau\gamma)e_q^{n+1} - \frac{\tau\varepsilon^2}{h^2}\left(e_{q+1}^{n+1} - 2e_q^{n+1} + e_{q-1}^{n+1}\right)\\
&= \underbrace{4\tau\gamma e_q^n + 2\tau\left(\theta_c - \frac{\theta}{1-\left(U_q^{n-1}\right)^2}\right)e_q^n} + \underbrace{e_q^{n-1} - 2\tau\gamma e_q^{n-1} + \frac{\tau\varepsilon^2}{h^2}\left(e_{q+1}^{n-1} - 2e_q^{n-1} + e_{q-1}^{n-1}\right)}\\
&\quad + 2\tau\left(\frac{\theta}{1-\left(U_q^{n-1}\right)^2} - \theta_c\right)e_q^{n-1}\\
&\quad + 2\tau\left[\left(\frac{\theta}{2}\ln\frac{1+U_q^{n-1}}{1-U_q^{n-1}} - \theta_c U_q^{n-1}\right) - \left(\frac{\theta}{2}\ln\frac{1+u_q^{n-1}}{1-u_q^{n-1}} - \theta_c u_q^{n-1}\right)\right]\\
&\quad + 2\tau\left[\left(\frac{\theta}{2}\ln\frac{1+u_q^{n-1}}{1-u_q^{n-1}} - \theta_c u_q^{n-1}\right) - \left(\frac{\theta}{2}\ln\frac{1+u_q^{n}}{1-u_q^{n}} - \theta_c u_q^{n}\right)\right]\\
&\quad + 2\tau\left(\frac{\theta}{1-\left(U_q^{n-1}\right)^2} - \theta_c\right)\left(u_q^n - u_q^{n-1}\right)\\
&\quad + 2\tau\gamma\left(u_q^{n+1} - 2u_q^n + u_q^{n-1}\right) + 2\tau\rho_q^n\\
&=: \sum_{i=1}^{8} K_i.
\end{aligned} \tag{4.3}$$

Taking the absolute value of both sides of (4.3) and using Lemma 2.1, we have the following:

$$\left|(1+2\tau\gamma)e_q^{n+1} - \frac{\tau\varepsilon^2}{h^2}\left(e_{q+1}^{n+1} - 2e_q^{n+1} + e_{q-1}^{n+1}\right)\right| \geq (1+2\tau\gamma)\left|e_q^{n+1}\right| = (1+2\tau\gamma)\left\|e^{n+1}\right\|_\infty. \tag{4.4}$$

For $|K_1|$, we can easily see that

$$|K_1| = 2\tau\left|2\gamma + \left(\theta_c - \frac{\theta}{1-\left(U_q^{n-1}\right)^2}\right)\right|\left|e_q^n\right| \leq 2\tau\left(2\gamma + \theta_c - \theta\right)\|e^n\|_\infty. \tag{4.5}$$

For $|K_2|$, we conclude the following:

$$|K_2| = \left|(1-2\tau\gamma)e_q^{n-1} + \frac{\tau\varepsilon^2}{h^2}\left(e_{q+1}^{n-1} - 2e_q^{n-1} + e_{q-1}^{n-1}\right)\right| \leq (1-2\tau\gamma)\left\|e^{n-1}\right\|_\infty, \quad \tau \leq \frac{h^2}{2(h^2\gamma+\varepsilon^2)}. \tag{4.6}$$

Using $|U_q^{n-1}| \leq \|U^{n-1}\|_\infty \leq \beta$, we obtain the following:

$$|K_3| = 2\tau\left|\frac{\theta}{1-\left(U_q^{n-1}\right)^2} - \theta_c\right|\left|e_q^{n-1}\right| \leq 2\tau\left(\frac{\theta}{1-\beta^2} - \theta_c\right)\left\|e^{n-1}\right\|_\infty. \tag{4.7}$$

Utilizing the differential mean value theorem, $|u| \le \beta$, and $|U_q^{n-1}| \le \|U^{n-1}\|_\infty \le \beta$, we can estimate $|K_4|$ as follows:

$$\begin{aligned} |K_4| &= 2\tau \left| \left(\frac{\theta}{2} \ln \frac{1+U_q^{n-1}}{1-U_q^{n-1}} - \theta_c U_q^{n-1} \right) - \left(\frac{\theta}{2} \ln \frac{1+u_q^{n-1}}{1-u_q^{n-1}} - \theta_c u_q^{n-1} \right) \right| \\ &= 2\tau \left| \left(\frac{\theta}{1-(\varphi^n)^2} - \theta_c \right) \left(U_q^{n-1} - u_q^{n-1} \right) \right| \\ &\le 2\tau \left(\frac{\theta}{1-\beta^2} - \theta_c \right) \left\| e^{n-1} \right\|_\infty, \end{aligned} \tag{4.8}$$

where φ^n is located between u_q^{n-1} and U_q^{n-1}, and $|\varphi^n| \le \beta$.

By the differential mean value theorem and $|u| \le \beta$, we obtain the following:

$$\begin{aligned} |K_5 + K_6| &= 2\tau \left| \left(\frac{\theta}{1-(\psi^n)^2} - \theta_c \right) \left(u_q^{n-1} - u_q^n \right) + \left(\frac{\theta}{1-\left(U_q^{n-1}\right)^2} - \theta_c \right) \left(u_q^n - u_q^{n-1} \right) \right| \\ &= 2\tau \left| \left(u_q^{n-1} - u_q^n \right) \left[\left(\frac{\theta}{1-(\psi^n)^2} - \theta_c \right) - \left(\frac{\theta}{1-\left(U_q^{n-1}\right)^2} - \theta_c \right) \right] \right| \\ &= 2\tau \left| \left(u_q^{n-1} - u_q^n \right) \left[\left(\frac{2\chi^n \theta}{\left(1-(\chi^n)^2\right)^2} \right) \left(\psi^n - U_q^{n-1} \right) \right] \right| \\ &\le 2\tau \left(\frac{2\theta\beta}{(1-\beta^2)^2} \right) |u_q^{n-1} - u_q^n| \left(|u_q^n - u_q^{n-1}| + |u_q^{n-1} - U_q^{n-1}| \right) \\ &\le \frac{4\tau\theta\beta}{(1-\beta^2)^2} \left| u_q^{n-1} - u_q^n \right|^2 + \frac{4\tau\theta\beta}{(1-\beta^2)^2} \left| u_q^{n-1} - u_q^n \right| e_q^{n-1} \\ &\le C(\theta,\beta)\tau^3 + \frac{8\tau\theta\beta^2}{(1-\beta^2)^2} \left\| e^{n-1} \right\|_\infty, \end{aligned} \tag{4.9}$$

where ψ^n is located between u_q^n and u_q^{n-1}, and χ^n is located between u_q^n and U_q^{n-1}.

For $|K_7|$ and $|K_8|$, we can obtain the following:

$$|K_7| + |K_8| \le 2\tau\gamma \left| u_q^{n+1} + u_q^{n-1} - 2u_q^n \right| + C(\varepsilon)\tau \left(\tau^2 + h^2 \right) \le C(\varepsilon,\gamma)\tau \left(\tau^2 + h^2 \right). \tag{4.10}$$

It follows from (4.4)–(4.10) that

$$\begin{aligned} (1+2\tau\gamma) \left\| e^{n+1} \right\|_\infty \le & \left(4\tau\gamma + 2\tau\theta_c - 2\tau\theta \right) \left\| e^n \right\|_\infty + \left(1 - 2\tau\gamma + \frac{4\tau\theta}{1-\beta^2} - 4\tau\theta_c + \frac{8\tau\beta^2\theta}{(1-\beta^2)^2} \right) \left\| e^{n-1} \right\|_\infty \\ & + C(\varepsilon,\theta,\gamma)\tau \left(\tau^2 + h^2 \right), \end{aligned}$$

namely,

$$\begin{aligned}(1+2\tau\gamma)\left(\left\|e^{n+1}\right\|_\infty-\left\|e^{n-1}\right\|_\infty\right)\leq\ & (4\tau\gamma+2\tau\theta_c-2\tau\theta)\left\|e^n\right\|_\infty+C(\varepsilon,\theta,\gamma)\tau\left(\tau^2+h^2\right)\\ &+\left(-4\tau\gamma+\frac{4\tau\theta}{1-\beta^2}-4\tau\theta_c+\frac{8\tau\beta^2\theta}{(1-\beta^2)^2}\right)\left\|e^{n-1}\right\|_\infty\\ &\leq 2\tau\left(2\gamma-\theta_c-\theta+\frac{2\theta}{1-\beta^2}+\frac{4\beta^2\theta}{(1-\beta^2)^2}\right)\left(\|e^n\|_\infty+\|e^{n-1}\|_\infty\right)\\ &+C(\varepsilon,\theta,\gamma)\tau\left(\tau^2+h^2\right).\end{aligned}$$

Then, we have the following:

$$\left\|e^{n+1}\right\|_\infty-\left\|e^{n-1}\right\|_\infty\leq 4\tau\left(2\gamma-\theta_c-\theta+\frac{2\theta}{1-\beta^2}+\frac{4\beta^2\theta}{(1-\beta^2)^2}\right)\left(\|e^n\|_\infty+\left\|e^{n-1}\right\|_\infty\right)+C\left(\varepsilon,\theta,\gamma\right)\tau\left(\tau^2+h^2\right).$$

We have the following:

$$\begin{aligned}\left(\left\|e^{n+1}\right\|_\infty+\|e^n\|_\infty\right)-\left(\|e^n\|_\infty+\left\|e^{n-1}\right\|_\infty\right)\leq\ & 4\tau\left(2\gamma-\theta_c-\theta+\frac{2\theta}{1-\beta^2}+\frac{4\beta^2\theta}{(1-\beta^2)^2}\right)\left(\|e^n\|_\infty+\left\|e^{n-1}\right\|_\infty\right)\\ &+C(\varepsilon,\theta,\gamma)\tau(\tau^2+h^2).\end{aligned}$$

Summing over n from 1 to $l-1$ ($2\leq l\leq M$), we derive the following:

$$\begin{aligned}\left\|e^l\right\|_\infty+\left\|e^{l-1}\right\|_\infty\leq\ & 4\tau\left(2\gamma-\theta_c-\theta+\frac{2\theta}{1-\beta^2}+\frac{4\beta^2\theta}{(1-\beta^2)^2}\right)\sum_{n=1}^{l-1}\left(\|e^n\|_\infty+\left\|e^{n-1}\right\|_\infty\right)\\ &+C\left(\varepsilon,\theta,\gamma,T\right)\tau\left(\tau^2+h^2\right)+\left\|e^1\right\|_\infty+\left\|e^0\right\|_\infty,\end{aligned}$$

namely,

$$\left\|e^l\right\|_\infty\leq 8\tau\left(2\gamma-\theta_c-\theta+\frac{2\theta}{1-\beta^2}+\frac{4\beta^2\theta}{(1-\beta^2)^2}\right)\sum_{n=1}^{l-1}\|e^n\|_\infty+C\left(\varepsilon,\theta,\gamma,T\right)\tau\left(\tau^2+h^2\right).\tag{4.11}$$

Notice that $e^0=0$ and $\|e^1\|_\infty\leq C(\varepsilon,\theta,\theta_c,\gamma,T)(\tau^2+h^2)$. Thus, we apply the discrete Grönwall inequality to (4.11) to obtain the desired estimate. This concludes the proof of the theorem.

5. Numerical experiments

In this section, we aim to substantiate our theoretical analysis with empirical examples. We employ the standard Newton method to solve Eq (2.3) and obtain the numerical solution at the first time level.

Example 1. We consider the 1D Allen–Cahn equation with the following initial value:

$$u_0(x)=0.25\sin(2\pi x),\forall x\in(0,1);$$

for other corresponding data, we set $\varepsilon=0.1$.

First, we test the convergence rate for discretization in time. Due to the absence of an analytical solution available for this numerical experiment, we define the errors of the numerical solution in the discrete norm L^∞ as $err = \|U^M - U^{2M}\|_\infty$. Moreover, letting $\theta = 1$ and $\theta_c = 2$, we have $\beta \approx 0.9575$. We display the errors with different τ in Tables 1 and 2. We find that the convergence orders of the errors are very close to 2. The approximate values of the theoretical error bounds, denoted as C_a, are also listed in Tables 1 and 2.

To verify the claimed second–order spatial accuracy, we consider the 1D periodic test with $u_0(x) = 0.25\sin(2\pi x)$, $\varepsilon = 0.1$, $\theta = 1$, $\beta \approx 0.9575$, and $\gamma = 50$. We refine $h \to h/2$ and take $\tau = Ch^2$ so that the temporal error is negligible. The error is measured by $\|U_h(T) - \mathcal{R}U_{h/2}(T)\|_\infty$, where $\mathcal{R}$ denotes the restriction from the fine grid to the coarse grid (in 1D, taking every other grid point). The observed rates are close to 2 (Table 3), thus confirming second–order spatial accuracy.

Example 2. We consider the 1D Allen–Cahn equation with the following initial value:

$$u_0(x) = 0.25\sin(2\pi x), \forall x \in (0, 1);$$

for other corresponding data, we set $\varepsilon = 0.1$.

Letting ($\gamma = 20$, $\theta = 4$, and $\theta_c = 7.7128$), ($\gamma = 1.3$, $\theta = 1.35$, and $\theta_c = 2.6031$), ($\gamma = 2$, $\theta = 1.6$, and $\theta_c = 3.0851$), and ($\gamma = 2$, $\theta = 1.5$, and $\theta_c = 2.9$), we have $\beta = 0.95$. These are consistent with the convergence results obtained in Theorem 4.1. Second, for $h = 1/50$, the maximum values of the numerical solutions with different τ are examined in Figures 1–4.

Remark 5.1. The restriction on the timestep in Theorem 3.2 is derived as a sufficient condition for the maximum bound principle. To illustrate this, we repeat the test in Figure 1 and choose larger timesteps $\tau = 0.01, 0.02$, and 0.03, which violate the theoretical bound. The maximum values of the numerical solutions with different τ are examined in Figure 5. In all these cases, the numerical solution still satisfies the maximum bound principle. This indicates that the theoretical timestep bound is sufficient but not sharp for this test setting.

Remark 5.2. Besides the nonlinear Crank–Nicolson initialization, we also tested a fully linear scheme at the first step as follows:

$$\frac{U^1 - U^0}{\tau} - \varepsilon^2 D_h\left(\frac{U^1 + U^0}{2}\right) = \frac{U^0 + U^1 - 3(U^0)^{.2}U^1 + (U^0)^{.3}}{2}.$$

In our numerical experiments (under the same settings as in Example 1), this linear initialization still preserves the maximum bound principle and does not deteriorate the observed second–order convergence behavior. Therefore, a fully linear first step can be employed in practice to avoid nonlinear iterations without compromising the performance in our tests.

Example 3. We consider the 2D Allen–Cahn equation with the following initial value:

$$u_0(x, y) = 0.5\sin(2\pi x)\cos(2\pi y) - 0.25, \forall\,(x, y) \in (0, 1)^2\,;$$

for other corresponding data, we set $\varepsilon = 0.01$.

First, we test the convergence rate for discretization in time. Due to the absence of an analytical solution available for this numerical experiment, we define the errors of the numerical solution in the discrete norm L^∞ as $err = \|U^M - U^{2M}\|_\infty$. Moreover, letting $\theta = 1$ and $\theta_c = 2$, we have $\beta \approx 0.9575$. We

display the errors with different τ in Tables 4 and 5. We find that the convergence orders of the errors are very close to 2.

Example 4. We consider the 2D Allen–Cahn equation with $\varepsilon = 0.01$ and the initial value

$$u_0(x, y) = 0.1\text{rand}(x, y) - 0.05, \forall\, (x, y) \in (0, 1)^2\,,$$

where we fix $h = 1/25$. First, we let $\gamma = 1$, and the corresponding numerical results with different τ are shown in Figures 6 and 7. Next, we let $\gamma = 2$, and the corresponding numerical results with different τ are shown in Figures 8 and 9. It is evident that the numerical solutions adhere to the maximum bound principle. Finally, we investigate the influence of fractional diffusion on the phase separation and coarsening process. The parameters are set as $h = 1/100$, $\tau = 1/100$, $\theta = 1$, $\theta_c = 2, \beta \approx 0.9575$, and different γ. Starting from random initial values, the snapshots of the numerical solutions at $t = 0$, 8, 16, 32, 50, and 100 are shown in Figures 10 and 11.

Example 5. We consider the 3D Allen–Cahn equation with $\varepsilon = 0.1$, and the initial value is defined by the following:

$$u_0(x, y, z) = 0.1\text{rand}(x, y, z) - 0.05, \forall\, (x, y, z) \in (-1, 1)^3\,,$$

where setting $\tau = 0.1$, $\gamma = 1$, $\theta = 1$, and $\theta_c = 2$ gives $\beta \approx 0.9575$. The three–dimensional simulation results are displayed in Figure 12, thus validating the effectiveness and stability of the proposed scheme in higher–dimensional problems.

Example 6. Since the numerical solution at the first time step is computed using the Crank–Nicolson (CN) scheme in this work, we compare the modified leapfrog scheme with the CN scheme in this example. We consider the 1D problem with the initial value $u_0(x) = 0.25\sin(2\pi x), \forall x \in (0, 1)$. For the parameter settings, we take $\theta = 1$, $\theta_c = 2$, $\gamma = 1$, $h = 1/800$, and $\varepsilon = 0.1$. We display the numerical errors with different τ in Table 6 under this set of parameter configurations. The results show that both schemes achieve the expected second–order temporal accuracy, while the proposed scheme consistently incurs a smaller Central Processing Unit (CPU) time for comparable errors.

Example 7. To examine whether taking a very large stabilization parameter deteriorates the accuracy, we consider the 1D problem with the initial value $u_0(x) = 0.25\sin(2\pi x), \forall x \in (0, 1)$. We fix the parameters as $\theta = 1$, $\theta_c = 2$, and $\varepsilon = 0.1$. For each γ, we perform a test in time by comparing solutions computed with $\tau = 1/10, 1/20, 1/40, 1/80$, and $1/160$, and report the observed temporal order. The results shown in Tables 7 and 8 indicate that the second–order temporal accuracy is maintained for all tested γ, while the error constant may mildly increase as γ becomes large.

Table 1. Numerical results with $\gamma = 1$ in 1D.

τ	$err\ (T = 1)$	Order	C_a	$err\ (T = 2)$	Order	C_a
1/10	8.926293e-04	–	0.0893	1.110847e-03	–	0.1111
1/20	2.353434e-04	1.9233	0.0941	2.770366e-04	2.0035	0.1108
1/40	6.005451e-05	1.9704	0.0961	6.931230e-05	1.9989	0.1109
1/80	1.514676e-05	1.9873	0.0969	1.734478e-05	1.9986	0.1109
1/160	3.802129e-06	1.9941	0.0973	4.338917e-06	1.9991	0.1111

Table 2. Numerical results with $\gamma = 2$ in 1D.

τ	$err\ (T = 1)$	Order	C_a	$err\ (T = 2)$	Order	C_a
1/10	1.676217e-03	–	0.1676	2.484848e-03	–	0.2485
1/20	4.507834e-04	1.8947	0.1803	6.254353e-04	1.9902	0.2502
1/40	1.156260e-04	1.9630	0.1850	1.571035e-04	1.9931	0.2514
1/80	2.920469e-05	1.9852	0.1869	3.938908e-05	1.9958	0.2521
1/160	7.334125e-06	1.9935	0.1878	9.862777e-06	1.9977	0.2525

Table 3. Numerical results with $\gamma = 50$ in 1D.

h	$\|U_h(T) - \mathcal{R}U_{h/2}(T)\|_\infty$	Order
1/100	3.787157e-05	–
1/200	9.469480e-06	1.9998
1/400	2.367469e-06	1.9999
1/800	5.918746e-07	2.0000
1/1600	1.479692e-07	2.0000

Table 4. Numerical results with $\gamma = 1$ in 2D.

τ	$err\ (T = 1)$	Order	$err\ (T = 2)$	Order
1/10	1.809449e-03	–	5.247341e-04	–
1/20	4.469939e-04	2.0172	1.431302e-04	1.8743
1/40	1.109548e-04	2.0103	3.671427e-05	1.9629
1/80	2.764807e-05	2.0047	9.154094e-06	2.0039
1/160	6.901611e-06	2.0022	2.276606e-06	2.0075

Table 5. Numerical results with $\gamma = 2$ in 2D.

τ	$err\ (T = 1)$	Order	$err\ (T = 2)$	Order
1/10	4.420168e-03	–	1.070465e-03	–
1/20	1.147633e-03	1.9454	2.123578e-04	2.3337
1/40	2.904692e-04	1.9822	5.500808e-05	1.9488
1/80	7.299952e-05	1.9924	1.377759e-05	1.9973
1/160	1.829485e-05	1.9964	3.434779e-06	2.0040

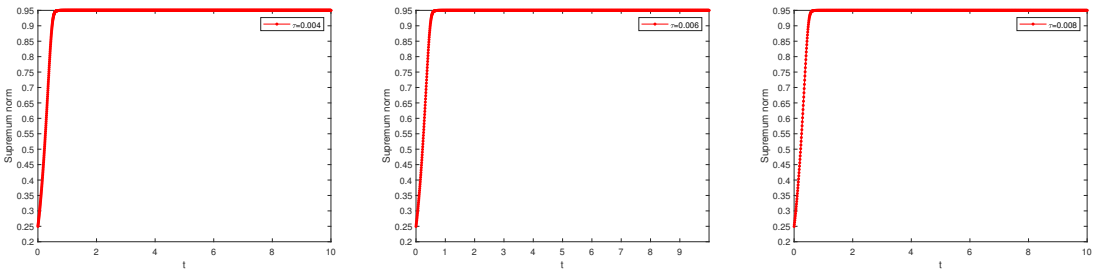

Figure 1. The maximum values of solution with $\gamma = 20$, $\theta = 4$, $\beta = 0.95$, and $\tau = 0.004, 0.006, 0.008$ (left to right, respectively).

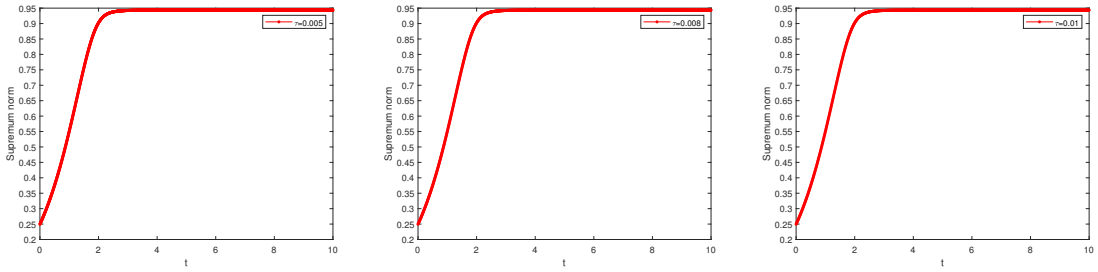

Figure 2. The maximum values of solution with $\gamma = 1.3$, $\theta = 1.35$, $\beta = 0.95$, and $\tau = 0.005, 0.008, 0.01$ (left to right, respectively).

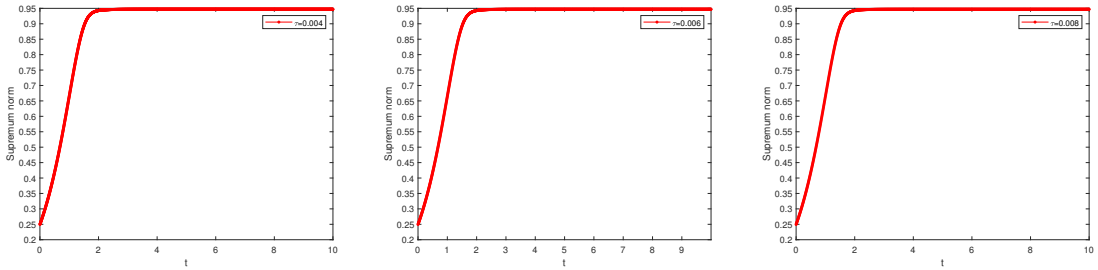

Figure 3. The maximum values of solution with $\gamma = 2$, $\theta = 1.6$, $\beta = 0.95$, and $\tau = 0.004, 0.006, 0.008$ (left to right, respectively).

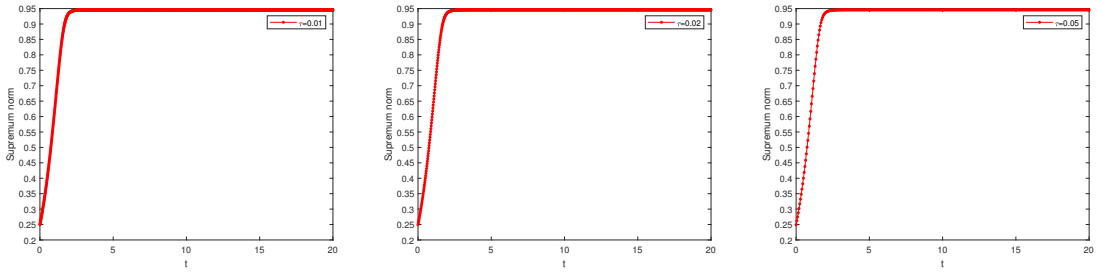

Figure 4. The maximum values of solution with $\gamma = 2$, $\theta = 1.5$, $\beta = 0.95$, and $\tau = 0.01, 0.02, 0.05$ (left to right, respectively).

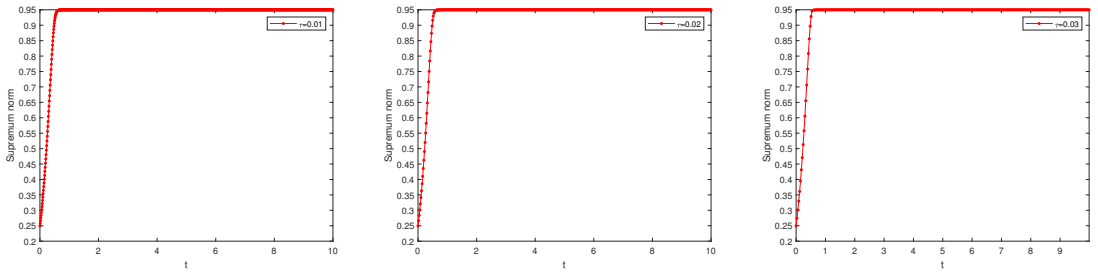

Figure 5. The maximum values of solution with $\gamma = 20$, $\theta = 4$, $\beta = 0.95$, and $\tau = 0.01, 0.02, 0.03$ (left to right, respectively).

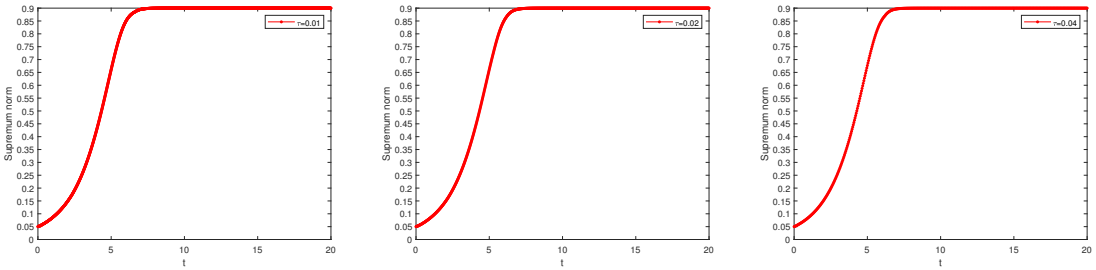

Figure 6. The maximum values of solution with $\gamma = 1, \theta = 1, \beta = 0.9$, and $\tau = 0.01, 0.02, 0.04$ (left to right, respectively).

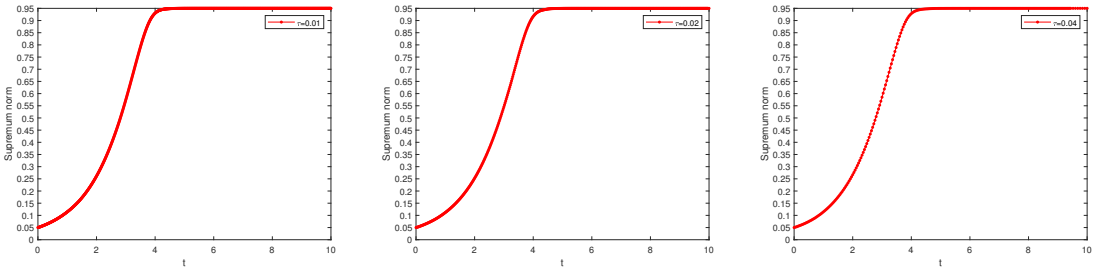

Figure 7. The maximum values of solution with $\gamma = 1$, $\theta = 1$, $\beta = 0.95$, and $\tau = 0.01, 0.02, 0.04$ (left to right, respectively).

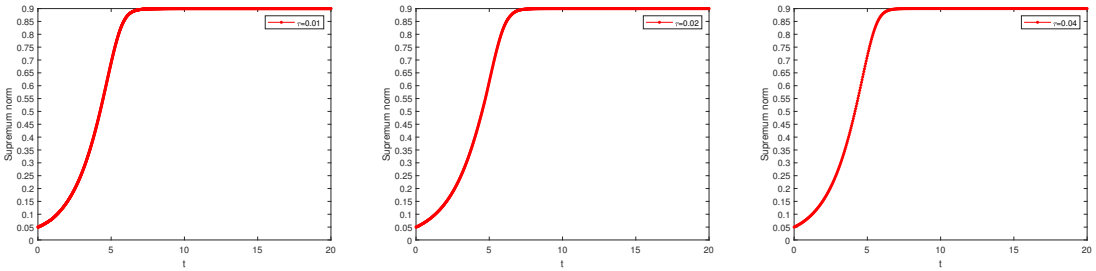

Figure 8. The maximum values of solution with $\gamma = 2, \theta = 1, \beta = 0.9$, and $\tau = 0.01, 0.02, 0.04$ (left to right, respectively).

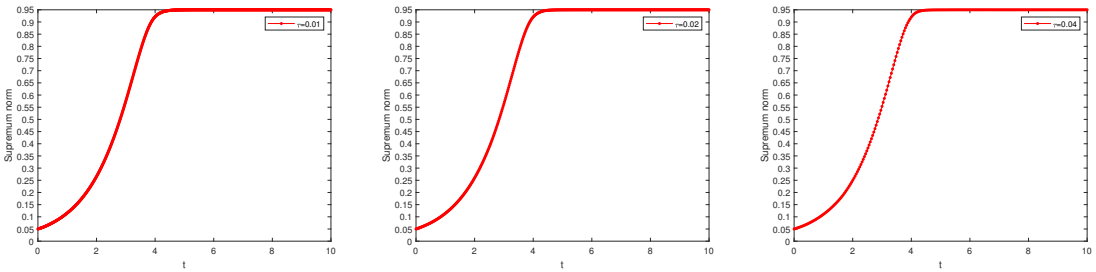

Figure 9. The maximum values of solution with $\gamma = 2$, $\theta = 1$, $\beta = 0.95$, and $\tau = 0.01, 0.02, 0.04$ (left to right, respectively).

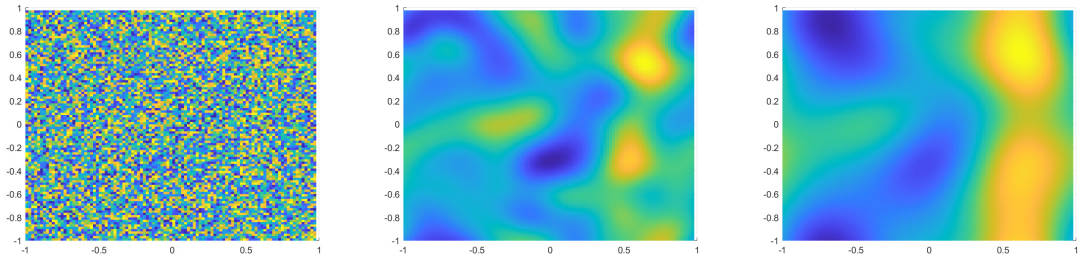

(a) t = 0 **(b)** t = 8 **(c)** t = 16

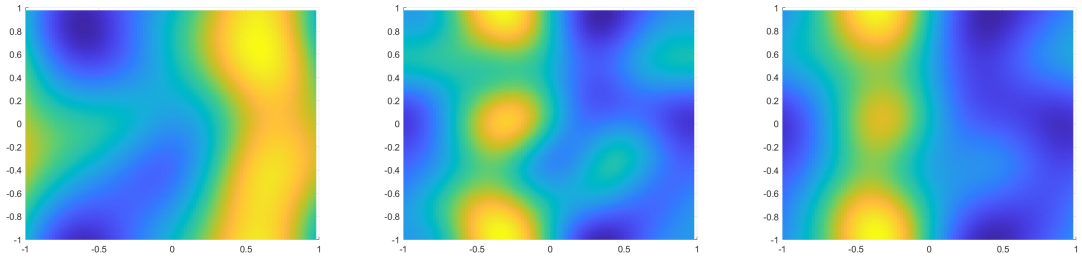

(d) t = 32 **(e)** t = 50 **(f)** t = 100

Figure 10. The snapshots of $t = 0, 8, 16, 32, 50$, and 100 when $\gamma = 1$.

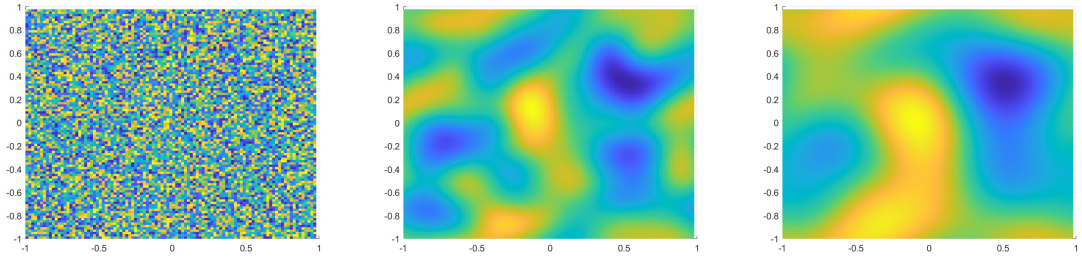

(a) t = 0 **(b)** t = 8 **(c)** t = 16

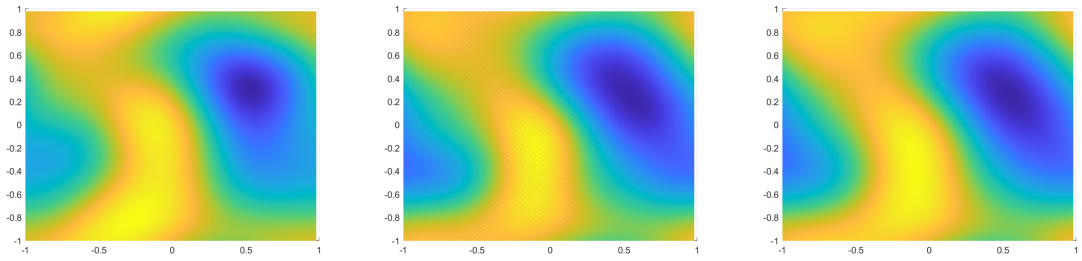

(d) t = 32 **(e)** t = 50 **(f)** t = 100

Figure 11. The snapshots of $t = 0, 8, 16, 32, 50$, and 100 when $\gamma = 2$.

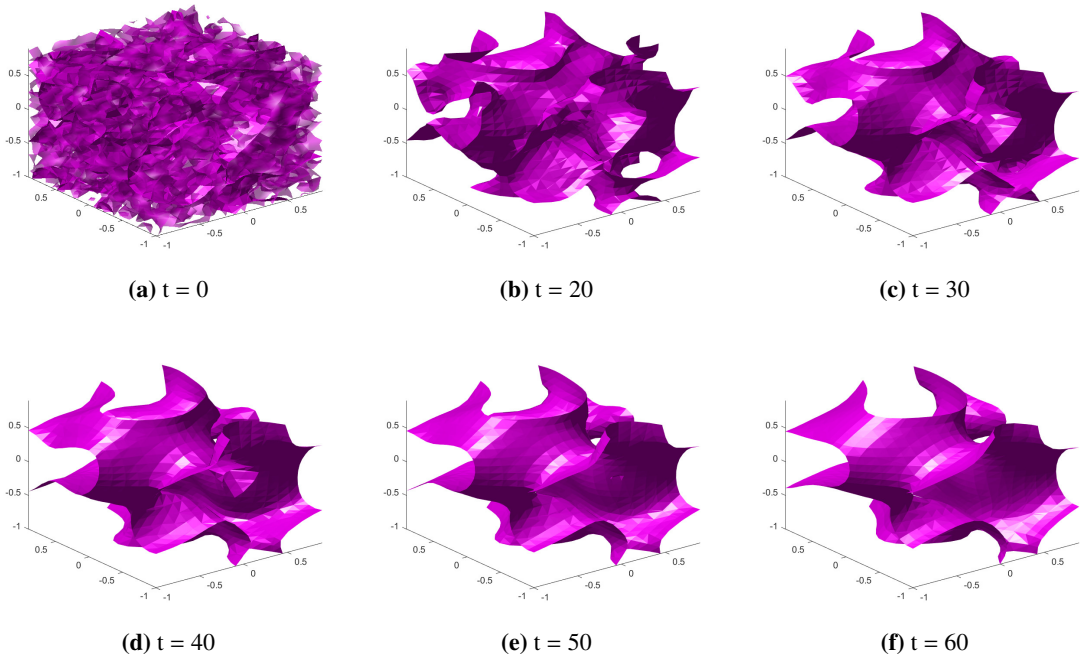

(a) t = 0 **(b)** t = 20 **(c)** t = 30

(d) t = 40 **(e)** t = 50 **(f)** t = 60

Figure 12. The snapshots of $t = 0, 20, 30, 40, 50$, and 60.

Table 6. Numerical results for modified leapfrog and CN schemes with $\gamma = 1$ in 1D.

	τ	err $(T = 1)$	Order	CPU time (s)
Modified leapfrog	1/10	8.926293e-04	–	0.288446
	1/20	2.353434e-04	1.9233	0.511799
	1/40	6.005451e-05	1.9704	0.957879
	1/80	1.514676e-05	1.9873	1.810452
	1/160	3.802129e-06	1.9941	3.598745
CN	1/10	8.289353e-05	–	0.466441
	1/20	2.084831e-05	1.9913	0.876361
	1/40	5.228757e-06	1.9954	1.659765
	1/80	1.309342e-06	1.9976	3.243381
	1/160	3.276089e-07	1.9988	6.372962

Table 7. Numerical results with different γ in 1D.

τ	err $(\gamma = 4)$	Order	err $(\gamma = 4.5)$	Order	err $(\gamma = 5)$	Order
1/10	3.130993e-03	–	3.472272e-03	–	3.804952e-03	–
1/20	8.740209e-04	1.8409	9.782437e-04	1.8276	1.081838e-03	1.8144
1/40	2.262822e-04	1.9495	2.538437e-04	1.9463	2.813642e-04	1.9430
1/80	5.729030e-05	1.9818	6.430522e-05	1.9809	7.131756e-05	1.9801
1/160	1.439628e-05	1.9926	1.616141e-05	1.9924	1.792637e-05	1.9922

Table 8. Numerical results with different γ in 1D.

τ	err ($\gamma = 10$)	Order	err ($\gamma = 20$)	Order	err ($\gamma = 30$)	Order
1/10	6.696534e-03	–	1.056858e-02	–	1.270546e-02	–
1/20	2.083894e-03	1.6841	3.912481e-03	1.4436	5.526160e-03	1.2011
1/40	5.543281e-04	1.9105	1.088183e-03	1.8462	1.606265e-03	1.7826
1/80	1.412985e-04	1.9720	2.804863e-04	1.9559	4.186471e-04	1.9399
1/160	3.556712e-05	1.9901	7.079985e-05	1.9861	1.059677e-04	1.9821

6. Conclusions

In this work, we directed our attention to the Allen–Cahn equation that involves logarithmic free energy, and put forward a finite difference scheme that achieves a second–order accuracy. The key design concept of this scheme lies in adopting a linearized modified form of the classical leapfrog scheme for temporal discretization, while pairing it with central differencing techniques for spatial discretization. To boost the numerical stability of the discrete framework, a second–order stabilization term was systematically integrated into the model structure. Through theoretical deductions, we revealed that as long as the time step size and stabilization parameter met appropriate constraint conditions, the obtained numerical solution will strictly comply with the discrete maximum bound principle. Moreover, we performed an in–depth stability analysis based on the L^∞ norm, and rigorously derived the corresponding error estimates for the scheme. To corroborate the validity and effectiveness of our theoretical conclusions, a series of numerical experiments were conducted, and the results confirmed the reliability of the proposed scheme. In conclusion, developing linear temporal schemes with enhanced accuracy orders that preserve the numerical maximum principle represents a promising direction for future research.

Use of AI tools declaration

The authors declare they have not used Artificial Intelligence (AI) tools in the creation of this article.

Conflict of interest

The authors declare there are no conflicts of interest.

References

1. S. M. Allen, J. W. Cahn, A microscopic theory for antiphase boundary motion and its application to antiphase domain coarsening, *Acta Metall.*, **27** (1979), 1085–1095. https://doi.org/10.1016/0001-6160(79)90196-2
2. A. Miranville, R. Quintanilla, A generalization of the Allen–Cahn equation, *IMA J. Appl. Math.*, **80** (2015), 410–430. https://doi.org/10.1093/imamat/hxt044
3. D. Jeong, S. Lee, D. Lee, J. Shin, J. Kim, Comparison study of numerical methods for solving the Allen–Cahn equation, *Comput. Mater. Sci.*, **111** (2016), 131–136. https://doi.org/10.1016/j.commatsci.2015.09.005

4. J. Shin, S. K. Park, J. Kim, A hybrid FEM for solving the Allen–Cahn equation, *Appl. Math. Comput.*, **244** (2014), 606–612. https://doi.org/10.1016/j.amc.2014.07.040
5. X. Yang, W. Zhao, W. Zhao, Optimal error estimates of a discontinuous Galerkin method for stochastic Allen–Cahn equation driven by multiplicative noise, *Commun. Comput. Phys.*, **36** (2024), 133–159. https://doi.org/10.4208/cicp.OA-2023-0280
6. W. Zhao, Q. Guan, Numerical analysis of energy stable weak Galerkin schemes for the Cahn–Hilliard equation, *Commun. Nonlinear Sci. Numer. Simul.*, **118** (2023), 106999. https://doi.org/10.1016/j.cnsns.2022.106999
7. X. Feng, A. Prohl, Numerical analysis of the Allen–Cahn equation and approximation for mean curvature flows, *Numer. Math.*, **94** (2003), 33–65. https://doi.org/10.1007/s00211-002-0413-1
8. X. Feng, H. Song, T. Tang, J. Yang, Nonlinear stability of the implicit–explicit methods for the Allen–Cahn equation, *Inverse Probl. Imaging*, **7** (2013), 679–695. https://doi.org/10.3934/ipi.2013.7.679
9. X. Feng, T. Tang, J. Yang, Stabilized Crank–Nicolson/Adams–Bashforth schemes for phase field models, *East Asian J. Appl. Math.*, **3** (2013), 59–80. https://doi.org/10.4208/eajam.200113.220213a
10. T. Tang, J. Yang, Implicit–explicit scheme for the Allen–Cahn equation preserves the maximum principle, *J. Comput. Math.*, **34** (2016), 451–461. https://doi.org/10.4208/jcm.1603-m2014-0017
11. T. Hou, H. Leng, Numerical analysis of a stabilized Crank–Nicolson/Adams–Bashforth finite difference scheme for Allen–Cahn equations, *Appl. Math. Lett.*, **102** (2020), 106150. https://doi.org/10.1016/j.aml.2019.106150
12. T. Hou, D. Xiu, W. Jiang, A new second–order maximum–principle preserving finite difference scheme for Allen–Cahn equations with periodic boundary conditions, *Appl. Math. Lett.*, **104** (2020), 106265. https://doi.org/10.1016/j.aml.2020.106265
13. Z. Xu, Y. Fu, Unconditional energy stability and maximum principle preserving scheme for the Allen–Cahn equation, *Numer. Algorithms*, **99** (2025), 355–376. https://doi.org/10.1007/s11075-024-01880-2
14. J. Shen, X. Yang, Numerical approximations of a Allen–Cahn and Cahn–Hilliard equations, *Discrete Contin. Dyn. Syst.*, **28** (2010), 1669–1691. https://doi.org/10.3934/dcds.2010.28.1669
15. T. Hou, T. Tang, J. Yang, Numerical analysis of fully discretized Crank–Nicolson scheme for fractional–in–space Allen–Cahn equations, *J. Sci. Comput.*, **72** (2017), 1214–1231. https://doi.org/10.1007/s10915-017-0396-9
16. M. Li, W. Li, Z. Du, T. Hou, A maximum bound principle preserving Crank–Nicolson/Adams–Bashforth finite difference scheme for Riesz space–fractional Allen–Cahn equations with logarithmic free energy, *Adv. Contin. Discrete Models*, **2025** (2025), 69. https://doi.org/10.1186/s13662-025-03929-5
17. C. Zheng, Z. Du, W. Kang, T. Hou, Two linearized maximum bound principle preserving finite difference schemes of Riesz space–fractional Allen–Cahn equations with logarithmic free energy, *Int. J. Comput. Math.*, **102** (2025), 2051–2077. https://doi.org/10.1080/00207160.2025.2533343
18. H. Zhang, J. Yan, X. Qian, X. Gu, S. Song, On the preserving of the maximum principle and energy stability of high–order implicit–explicit Runge–Kutta schemes for the space–fractional Allen–Cahn equation, *Numer. Algorithms*, **88** (2021), 1309–1336. https://doi.org/10.1007/s11075-021-01077-x

19. B. Zhang, Y. Yang, Efficient structure–preserving scheme for the space fractional Allen–Cahn equation with logarithmic Flory–Huggins potential, *J. Sci. Comput.*, **103** (2025), 18. https://doi.org/10.1007/s10915-025-02832-1

20. Y. He, W. Sun, Stability and convergence of the Crank–Nicolson/Adams–Bashforth scheme for the time–dependent Navier–Stokes equations, *SIAM J. Numer. Anal.*, **45** (2007), 837–869. https://doi.org/10.1137/050639910

21. Y. He, The Crank–Nicolson/Adams–Bashforth scheme for the time–dependent Navier–Stokes equations with nonsmooth initial data, *Numer. Methods Partial Differ. Equations*, **28** (2012), 155–187. https://doi.org/10.1002/num.20613

22. Y. Huang, W. Yang, H. Wang, J. Cui, Adaptive operator splitting finite element method for Allen–Cahn equation, *Numer. Methods Partial Differ. Equations*, **35** (2019), 1290–1300. https://doi.org/10.1002/num.22350

23. J. Park, C. Lee, Y. Choi, H. G. Lee, S. Kwak, Y. Hwang, et al., An unconditionally stable splitting method for the Allen–Cahn equation with logarithmic free energy, *J. Eng. Math.*, **132** (2022), 18. https://doi.org/10.1007/s10665-021-10203-6

24. C. Li, Y. Huang, N. Yi, An unconditionally energy stable second order finite element method for solving the Allen–Cahn equation, *J. Comput. Appl. Math.*, **353** (2019), 38–48. https://doi.org/10.1016/j.cam.2018.12.024

25. J. Yang, N. Yi, H. Zhang, High–order, unconditionally maximum–principle preserving finite element method for the Allen–Cahn equation, *Appl. Numer. Math.*, **188** (2023), 42–61. https://doi.org/10.1016/j.apnum.2023.03.002

26. F. Nudo, Two one–parameter families of nonconforming enrichments of the Crouzeix–Raviart finite element, *Appl. Numer. Math.*, **203** (2024), 160–172. https://doi.org/10.1016/j.apnum.2024.05.023

27. F. Nudo, A general quadratic enrichment of the Crouzeix–Raviart finite element, *J. Comput. Appl. Math.*, **451** (2024), 116112. https://doi.org/10.1016/j.cam.2024.116112

28. F. Dell'Accio, A. Guessab, F. Nudo, New quadratic and cubic polynomial enrichments of the Crouzeix–Raviart finite element, *Comput. Math. Appl.*, **170** (2024), 204–212. https://doi.org/10.1016/j.camwa.2024.06.019

AIMS Press